Title

Block Liposomes from Curvature-Stabilizing Lipids: Connected Nanotubes, -rods, or -spheres

Journal

Langmuir, 25(5)

ISSN

0743-7463

Authors

Zidovska, Alexandra

Ewert, Kai K

Quispe, Joel

et al.

Publication Date

2009-03-03

DOI

10.1021/la8022375

Published in final edited form as:
Langmuir. 2009 March 3; 25(5): 2979–2985. doi:10.1021/la8022375.

Block Liposomes from Curvature-Stabilizing Lipids:

Connected Nanotubes, -rods or -spheres

Alexandra Zidovska[1], **Kai K. Ewert**[1], **Joel Quispe**[2], **Bridget Carragher**[2], **Clinton S. Potter**[2], and **Cyrus R. Safinya**[1,*]

1*Materials, Physics, and Molecular, Cellular and Developmental Biology Departments, University of California at Santa Barbara, Santa Barbara, CA 93106*

2*National Resource for Automated Molecular Microscopy, Department of Cell Biology, The Scripps Research Institute, 10550 North Torrey Pines Road, La Jolla, CA 92037, USA*

Abstract

We report on the discovery of block liposomes, a new class of chain-melted (liquid) vesicles, with membranes comprised of mixtures of the membrane curvature stabilizing multivalent lipid MVLBG2 of colossal charge +16 e and neutral 1,2-dioleoyl-*sn*-glycero-3-phosphatidylcholine (DOPC). In a narrow MVLBG2 composition range (8-10 mol %), cryo-TEM revealed the block liposomes consisting of distinctly shaped, yet connected, nanoscale spheres, pears, tubes, or rods. Unlike typical liposome systems, where spherical vesicles, tubular vesicles, and cylindrical micelles are separated on the macroscopic scale, within a block liposome, shapes are separated on the nanometer scale. Diblock (pear-tube) and triblock (pear-tube-pear) liposomes contain nanotubes with inner lumen diameter 10-50 nm. Diblock (sphere-rod) liposomes were found to contain micellar nanorods ≈ 4 nm in diameter and several μm in length, analogous to cytoskeletal filaments of eukaryotic cells. Block liposomes may find a range of applications in chemical and nucleic acid delivery and as building blocks in the design of templates for hierarchical structures.

Keywords

block liposomes; lipid bilayer; curvature-stabilizing lipids; membrane curvature

Introduction

Lipids - one of the main building blocks of life - and their assemblies (e.g. membranes and liposomes) play a major role in numerous cellular processes including compartmentalization, macromolecular transport, and signal transduction[1]. A distinguishing feature of membranes *in vivo*, enabling their function, is the evolution in their shapes[2-5]. Much effort has been expended to elucidate membrane shapes in the context of their interactions with membrane-associated, curvature generating and stabilizing proteins[2-4,6] and lipids[7,8]. Examples include (i) vesicle budding, such as in receptor-mediated endocytosis, in inter-organelle trafficking and at synaptic junctions recycling vesicles, (ii) neuronal process formation, and (iii) membrane shape evolution in dividing cells during cytokinesis[1,2]. A recent in vitro study led to the observation of spontaneous formation of lipid tubules upon addition of brain derived curvature generating lipids[8]. While a large variety of micron scale vesicle shapes including spheres, ellipsoids and oblates, tori, and discocytes and stomatocytes has been described previously[9-13], the discovery of block liposomes (BLs) presents a major challenge to the

*Email: safinya@mrl.ucsb.edu

current understanding of membrane shapes at equilibrium. Current theories, based on the widely accepted Helfrich elastic free energy of membranes[14], predict macroscopically phase separated distinctly shaped liposomes[9,10,15]. In contrast, shapes are connected and separated on the nanometer scale in block liposomes. New theories of charged membranes are required to account for block liposomes.

To elucidate the role of high membrane curvature forming lipids on vesicle shape, we explored the behavior of spherical DOPC liposomes in the presence of MVLBG2 and discovered a remarkable new class of liquid (chain-melted) vesicles. MVLBG2 is a multivalent cationic lipid with a di-oleyl tail and a dendritic headgroup carrying a colossal charge of +16 e at full protonation[16] (See Fig. 1 S in the Supporting Information (SI) for the chemical structure of MVLBG2 and molecular models of MVLBG2 and DOPC). The extreme mismatch in headgroup area versus tail area leads to a cone shape of the molecule (Fig. 1 S). In contrast, the charge-neutral zwitterionic DOPC has a cylindrical molecular shape. In a narrow composition range (8-10 mol % MVLBG2), differential-interference-contrast-microscopy (DIC) revealed an evolution in vesicle shapes on the micrometer scale from spherical to a new class of vesicles, named block liposomes, comprised of distinctly shaped connected liquid liposomes (Fig. 1 A-C). This novel morphology persists down to the nanometer scale as revealed by cryogenic transmission electron microscopy (cryo-TEM). Diblock (pear-tube) liposomes (Fig. 1 A) and triblock (pear-tube-pear) liposomes (Fig. 1 B) contain tubules of diameter 10-50 nm and length >1μm. These block liposomes are the first examples of synthetic lipid systems containing tubular vesicles in the liquid phase with the inner lumen in the true nanometer scale range. A spontaneous topological transition from tubes (cylindrical vesicles) to rods (cylindrical micelles) leads to the formation of a coexisting population of diblock (sphere-rod) liposomes (Fig. 1 C).

Materials and Methods

Materials

DOPC was purchased from Avanti Polar Lipids. MVLBG2 was synthesized as described[16].

Lipid Solutions

Solutions of MVLBG2 trifluoroacetate were prepared in chloroform/methanol (9:1, v/v). Lipid solutions were combined at the desired ratio of lipids and dried, first by a stream of nitrogen and subsequently in a vacuum for 8 to 12 hours. To the residue, high resistivity (18.2 MΩcm) water was added and the mixture incubated at 37 °C for at least 12 hours to give a final concentration of 10 mg/mL (30 mg/mL for micellar solutions). The lipid solutions were stored at 4 °C until use. The lipids remained in their chain-melted liquid state due to their unsaturated lipid tails. This was confirmed by wide angle X-ray scattering experiments (data not shown). The pH of aqueous lipid solutions was measured using indicator paper (due to the small sample volume) as 5.5 ± 0.5, which corresponds to an average MVLBG2 charge of +14.5 e to +16 e.

Optical Microscopy

A Nikon Diaphot 300 inverted microscope equipped for epifluorescence and DIC and a SensiCam^{QE} High Speed digital camera were used. For fluorescence microscopy, liposome solutions were prepared at 1 mmol with 1 mol % lipid dye Texas Red® DHPE (Molecular Probes).

Cryo-TEM

The specimens were preserved in a layer of vitreous ice suspended over a holey carbon substrate. The holey carbon films consist of a thin layer of pure carbon fenestrated by 2 μm

holes spaced 4 μm apart and suspended over 400 mesh copper grids[17]. The grids were cleaned prior to vitrification with a Solarus plasma cleaner (Gatan Inc.) using a 25% O_2, 75% Ar mixture. The concentration of the sample solution was varied depending on the kind of the sample, typically 5-10 mg/mL for aqueous lipid solutions and 30 mg/mL for the micellar lipid solutions. Samples were vitrified by plunge freezing into liquid ethane using a Vitrobot (FEI Co.). Microscopy was carried out using a Tecnai F20 (FEI Co.) TEM at 120 keV with magnifications ranging from 29,000-280,000. Images were acquired at an underfocus of ~2.5 μm to a slow scan CCD camera (TVIPS GmbH) using the Leginon software system[18].

Results and Discussion

Figure 2 (A-G) displays DIC images of the MVLBG2/DOPC/water system undergoing phase transitions as a function of its composition. The membrane mixtures poor in MVLBG2 show polydisperse multilamellar vesicles for 0-8 mol % MVLBG2 (Fig. 2 A), which are reentrant between 12-50 mol % MVLBG2 (Fig. 2, D and E). A phase consisting of block liposomes enters in a very narrow composition interval of ≈8-10 mol % MVLBG2 (Fig. 2 B). Its hallmark is the ≈5 μm long cylindrical core of diameter ≈0.5 μm, capped with quasi-spherical vesicles with diameter of a few μm at both its ends (Fig. 2 C). Tapping mode AFM experiments show that these micrometer-scale structures are multilamellar (Fig. 2 J and K). With increasing MVLBG2 content in the sample, the system reenters the polydisperse multilamellar vesicle regime (Fig. 2 D). Then, at ≈25 mol %, the system transforms into a nearly monodisperse population of spherical vesicles with diameter ≈2 μm (Fig. 2 E). With further increase of MVLBG2 content, a macroscopic coexistence of micelles and vesicles sets in around 50 mol % MVLBG2 (Fig. 2 F). At MVLBG2 contents above 75 mol %, only micelles (not seen in DIC) populate the system (Fig. 2 G). Fluorescence imaging (Fig. 2 H) proves their existence, and cryo-TEM (Fig. 2 I) elucidates their size and morphology.

A series of cryo-TEM images are shown in Fig. 3, which demonstrate that the block liposomes (8-10 mol % MVLBG2) persist down to the nanometer scale and reveal the detailed features of typical di- and triblock liposomes containing tubular sections. Two triblock (pear-tube-pear) liposomes (with vesicles of asymmetric size capping the tube) can be seen in Fig. 3 A. The high-magnification image in the inset shows that the tubular section has an inner lumen diameter of ≈10 nm (Fig. 3 B; the white arrowheads point out the thickness of a single bilayer ≈4 nm). A diblock (pear-tube) liposome with inner diameter of ≈50 nm is seen in Fig. 3 C. We frequently observe one block liposome encapsulated within another block liposome (Fig. 3 D and 3 E (top arrow)). In these cases, the inner, smaller diameter tubule protrudes through the encapsulating membrane, demonstrating its high bending rigidity. Fig. 3 E also shows a diblock liposome (bottom arrow) and several block liposomes (second, third, and fourth arrows from bottom), which are either di- or triblocks (See Fig. 2 S in the SI for a nearly symmetric triblock (pear-tube-pear) liposome, which was partially broken in the cryo-preparation). Schematics of these typical block liposomes containing tubular sections and their internal architecture based on the hypothesized mechanism of their formation (cf. Fig. 5) are shown in Fig. 3 F. The abundance of these structures in the sample is demonstrated in Fig. 5 S in the SI.

Intriguingly, block liposomes containing tubular sections coexist with another block liposome type, which contains a highly rigid lipid nanorod section comprised of cylindrical micelles. Figure 4 (A-D) shows typical images of these remarkable diblock (sphere-rod) liposomes which demonstrate that the micellar nanorods remain attached to the spherical vesicles. Their diameter equals the thickness of a lipid bilayer (≈4 nm, corresponding to the hydrophobic core of the rod with high contrast in cryo-TEM) and their length can reach up to several μm, corresponding to an aspect ratio of the order of 1000. A lower magnification image (Fig. 4 D) shows a collection of these block liposomes with different spherical vesicle sizes. Schematics of this novel block liposome structure based on the hypothesized mechanism of their formation

(cf. Fig. 7) are shown in Fig. 4 E. The region where the lipid nanorod is anchored to the lipid bilayer spherical vesicle is a true mathematical singularity analogous to the core of a liquid crystal (-1/2) disclination[19].

As we now describe, the key parameters leading to the formation of block liposomes containing tubular sections are the conically shaped cationic MVLBG2 and its counterions, which, when mixed with cylindrically shaped DOPC, allows for the breaking of symmetry between the inner and outer monolayers. This leads to a positive spontaneous curvature C_0 of the membrane (Fig. 5 A). We hypothesize that there are three possible pathways for the formation of a triblock liposome (pear-tube-pear), shown schematically in Fig. 5 B. Two pathways are due to the coupling between thermally induced bending modes and compositional fluctuations. Along pathway (i), a compositional fluctuation leading to a region with a high concentration of MVLBG2 (green), coupled to a curvature fluctuation, drives the formation of a tubular high curvature region. Alternatively, along (ii), a bending mode fluctuation producing a high curvature region coupled to a compositional fluctuation will drive the formation of the tubule section with MVLBG2 segregated to the regions of the tubule with high positive curvature[20]. Bending fluctuations are readily observed with optical microscopy (cf. Fig. 2 A). The final result of either pathway is the formation of a high curvature tubular section. Our observation of tubular regions has to imply that locally, in these regions, the spontaneous curvature is large and of the order of the observed curvature $C_0 \approx C > 0$ (otherwise the elastic cost of formation of tubes $\approx \kappa(C\text{-}C_0)^2$, where κ is the bending rigidity of a bilayer, would be prohibitive because the observed high persistence length of the tubes implies that $\kappa/k_BT \gg 1$). The mechanism leading to $C_0 > 0$ in the tubule region in this 2-component system, with $C_0^{MVLBG2} > 0$ and $C_0^{DOPC} = 0$, is a spontaneous breaking of symmetry between the inner and outer leaflet, with a higher concentration of MVLBG2 in the outer layer because of its intrinsic positive C_0. The third mechanism that could lead to a breaking of symmetry between the inner and outer leaflet of the bilayer in a 2-component system leading to $C_0 > 0$ would be a curvature fluctuation coupled to a non-symmetrical distribution of counterions between the outside and the inside of the bilayer (Fig. 5 B (iii)). Thus, in addition to the asymmetry in composition between the outer and inner layer giving rise to C_0, the spontaneous curvature may also be, in part, due to a larger concentration of counterions near the inner layer. The diblock liposomes may form by the same process with the initial fluctuations (membrane shape instability) to regions of high curvature occurring as a result of membrane protrusions and where a sufficiently large protrusion may be stabilized by the influx of MVLBG2. Neither element sensitive electron microscopy nor fluorescence imaging allows one to observe the breaking of compositional symmetry between the inner and outer leaflet, since these techniques only yield a projection image of the observed structure.

A clue to the mechanism leading to nanorod formation can be seen in Fig. 6 A, which displays cryo-TEM images of nanotube-nanorod transition regions within a block liposome. The white arrows are pointing towards the loci of ongoing transition processes, clearly displaying the drastic change in diameter. The mechanism we propose for this transition is schematically depicted in Fig. 7. As described earlier, the nanotube section contains more MVLBG2 lipids in the outer layer (Fig. 7 (i)). The process starts by a fluctuation towards a region with even higher curvature, bringing two opposing bilayers of the tube into close proximity (Fig. 7 (ii)). The fluctuation in the tube would require a local composition fluctuation which allows for locally softer regions (with a lower density of MVLBG2). This higher curvature will induce a lateral phase separation within the tube section where MVLBG2 will tend to diffuse to the higher-curvature region (dark green arrows) while DOPC will tend to diffuse in the opposite direction (yellow arrows, outer monolayer), towards the lower-curvature region of the tubule. At the same time, the DOPC lipids in the inner monolayer of this transiently formed higher-curvature region will also tend to diffuse away from this region with highly negative curvature towards the tubular region with much lower curvature (yellow arrows, inner monolayer, Fig.

7 (ii)). The topological phase transition from nanotube to nanorod requires a fusion event between opposing inner monolayers of the nanotube as depicted in Fig. 7 (iii). The region of fusion is in the immediate vicinity of the nucleation and growth site for nanorod formation (Fig. 7 (iii) (inset) and (iv)). The final nanorod section, which has a larger concentration of MVLBG2 in the outer monolayer compared to the tube section (consistent with the larger curvature of the rod), is also a longer region due to the conservation of the total area of the lipids before and after the tube-rod transition (Fig. 7 (v)). Stable complexes of nanorods and DNA have recently been observed in the H_I^C phase of DNA complexes of a lipid mixture consisting of 25 mol % MVLBG2 and 75 mol % DOPC[16]. This supports our hypothesis that MVLBG2 laterally phase separates in the diblock (sphere-rod) liposomes described here where the MVLBG2 composition is between 8 and 10 mol%.

The fusion is expected to stop when most of the MVLBG2 molecules have been used up to make the nanorod sections. This would leave mostly DOPC lipids for the vesicles capping the rods. This proposed model of the tube-rod transition is consistent with the vast majority of the cryo-TEM images of nanorod-containing block liposomes being devoid of a tubular section, with the rods directly connected to spherical vesicles (Fig. 4, A-D). Fig. 6 A justifies the model by the unambiguous presence of “bubbles”, where the fusion process has occurred on either side. Furthermore, Fig. 6 (B and C) shows a rare cryo-TEM image of what appears to be an intermediate phase of a tube-containing block liposome, where the tube-rod transition process is only partially complete with the rod attached to a tubular section (which still contains MVLBG2) rather than a spherical vesicle which would be rich in DOPC and nearly devoid of MVLBG2.

We expect that the tubular and rod regions of BLs, which are rich in MVLBG2 will also be regions with very high counterion condensation (i.e. allowing neighboring charged headgroups to pack). This is consistent with recent theory for inhomogeneous charged membranes (mimicking membranes containing multivalent lipids), which show a significant relative increase in the concentration of counterions bound to regions of high charge, compared to bound counterions for a homogeneous charged membrane with the same average charge density[21]. Counterions cause only partial neutralization and the remaining charge gives rise to an increase in the effective stiffness leading to a large persistence length of nanotubes and nanorods.

Fig. 8 A shows a rare example of a vesicle membrane shape evolving from a sphere to a sphere with four protruding symmetrical processes mimicking a clover leaf with four leaflets (instead of the more typical single process leading to the diblock (pear-tube) liposome). To unequivocally demonstrate that electrostatic forces resulting from the conically shaped, charged lipid MVLBG2 are the driving force in the creation of the block liposomes, we studied block liposomes at high salt conditions (250 mM NaCl, Debye length 0.6 nm, effectively screening the electrostatic forces). Block liposomes are not stable under these conditions and are replaced by the usual multilamellar vesicles with spherical topology (Fig. 8 B). Current state-of-the-art analytical theories[10] and simulations of membrane shapes[22], which incorporate coupling between curvature and composition, are not able to predict our experimentally discovered block liposomes comprised of distinctly shaped liposomes, which remain connected. This may be due to the omission of electrostatic forces in current theories and simulations, which are key to the formation of block liposomes. New theories of charged membranes are required to describe block liposomes.

Figure 9 (A and B) plots the results of a statistical analysis of the nanotube and nanorod populations, including the diameter distribution within the tube population. The diameter histograms weighted by the surface area—indicative of the real amount of material in the nanorod and nanotube state—and by the length of the structure—manifesting the striking

length of nanorods compared to nanotubes—are shown in Figures 9 A and 9 B, respectively. The cryo-TEM images of block liposomes, with time intervals between the preparation and vitrification as long as two months (see Table 1 S in the SI), show that these are robust, long-lived structures. DIC experiments also show that the μm-scale multilamellar block liposomes are long-lived on time scales of over a year. If the block liposomes were not equilibrium structures, it is reasonable to assume that we would have also observed macroscopic phase separation of cylindrical micelles (nanorods) and spherical vesicles. However, the analysis of 426 cryo-TEM images of block liposomes did not show even a single instance of an individual cylindrical micelle. While these observations suggest that BLs are equilibrium structures we cannot rule out the possibility that they are kinetically trapped structures with barriers much larger than the thermal energy.

Conclusions

The discovery of block liposomes demonstrates that the addition of a single type of "electrostatic force generating conically shaped molecule" to neutral vesicles leads to a membrane shape evolution with long-lived robust structures which are remarkably similar to what is seen *in vivo* (e.g. cytokinesis in cell division, tubular neuronal processes, and tubules extending from the endoplasmic reticulum), where the much more complex out-of-equilibrium processes all require multiple distinct biomolecules working in concert and consuming the energy of hydrolysis. A recent report also described the formation of tubules upon addition of ganglioside lipids with large headgroups to DOPC containing vesicles in presence of salt[8]. The analogy with membrane shape evolution may also extend to the flow of certain abstract geometric shapes in topology which follows the "Ricci flow equation" used to describe surfaces where regions of high curvature diffuse into lower curvature regions (e.g. to generate the flow of shapes from a sphere (positive curvature) to a dumbbell-shaped surface, containing negative curvature regions)[23,24]. The nanotubes and nanorods make desirable candidates for drug/gene delivery applications [25-32] or as template for nanostructures such as wires or needles. Future studies involving systematic variations in the shape, size and charge of the curvature-stabilizing lipid (which mimics curvature stabilizing proteins *in vivo*) will lead to optimal control of the tubule diameter distribution. Finally, one should be able to produce analogous block polymersomes in mixtures of charged and neutral co-polymers[33] or peptides[34].

Supplementary Material

Refer to Web version on PubMed Central for supplementary material.

Acknowledgement

We are indebted to Sandy Schmid for making us aware of the curvature generating proteins. We further acknowledge useful discussions with Sam Safran and Didier Roux. This work is supported by DOE grant DE-FG02-06ER46314, NIH grant GM-59288, NSF grant DMR-0803103, and ONR No. N00014-05-1-0540. Some of this research was conducted at the National Resource for Automated Molecular Microscopy which is supported by the NIH National Center for Research Resources P41 program.

References

(1). Alberts, B. Molecular Biology of The Cell. Vol. 4th ed.. Garland Science; New York: 2002.

(2). McMahon HT, Gallop JL. Nature 2005;438:590–596. [PubMed: 16319878]

(3). Parthasarathy R, Groves JT. Soft Matter 2007;3:24–33.

(4). Roux A, Cuvelier D, Nassoy P, Prost J, Bassereau P, Goud B. EMBO J 2005;24:1537–1545. [PubMed: 15791208]

(5). Qi SY, Groves JT, Chakraborty AK. Proc. Natl. Acad. Sci. U.S.A 2001;98:6548–6553. [PubMed: 11371622]

(6). Hinshaw JE, Schmid SL. Nature 1995;374:190–192. [PubMed: 7877694]
(7). Israelachvili JN, Mitchell DJ, Ninham BW. Journal of the Chemical Society-Faraday Transactions II 1976;72:1525–1568.
(8). Akiyoshi K, Itaya A, Nomura SM, Ono N, Yoshikawa K. FEBS Lett 2003;534:33–38. [PubMed: 12527358]
(9). Lipowsky, R.; Sackmann, E. Structure and Dynamics of Membranes. Vol. 1A. Elsevier; Amsterdam: 1995.
(10). Seifert U. Advances in Physics 1997;46:13–137.
(11). Chiruvolu S, Warriner HE, Naranjo E, Idziak SHJ, Raedler JO, Plano RJ, Zasadzinski JA, Safinya CR. Science 1994;266:1222–1225. [PubMed: 7973704]
(12). Yuan J, Parker ER, Hirst LS. Langmuir 2007;23:7462–7465. [PubMed: 17555339]
(13). Danino D, Bernheim-Groswasser A, Talmon Y. Colloids and Surfaces a-Physicochemical and Engineering Aspects 2001;183:113–122.
(14). Helfrich W. Z. Naturforsch., C: Biosci 1973;C 28:693–703.
(15). Safran, SA. Statistical Thermodynamics of Surfaces, Interfaces, and Membranes. Westview Press; 1994.
(16). Ewert KK, Evans HM, Zidovska A, Bouxsein NF, Ahmad A, Safinya CR. J. Am. Chem. Soc 2006;128:3998–4006. [PubMed: 16551108]
(17). Quispe J, Damiano J, Mick SE, Nackashi DP, Fellmann D, Ajero TG, Carragher B, Potter CS. Microsc. microanal 2007;13:365–371. [PubMed: 17900388]
(18). Suloway C, Pulokas J, Fellmann D, Cheng A, Guerra F, Quispe J, Stagg S, Potter CS, Carragher B. J. Struct. Biol 2005;151:41–60. [PubMed: 15890530]
(19). de Gennes, PG.; Prost, J. The Physics of Liquid Crystals. Oxford University Press; 1993.
(20). Sackmann E. FEBS Lett 1994;346:3–16. [PubMed: 8206154]
(21). Lukatsky DB, Safran SA, Lau AWC, Pincus P. Europhys. Lett 2002;58:785–791.
(22). Reynwar BJ, Illya G, Harmandaris VA, Muller MM, Kremer K, Deserno M. Nature 2007;447:461–464. [PubMed: 17522680]
(23). Mackenzie D. Science 2006;314:1848–1849. [PubMed: 17185565]
(24). Collins GP. Sci. Am 2004;291:94–103. [PubMed: 15255593]
(25). Raviv U, Needleman DJ, Li YL, Miller HP, Wilson L, Safinya CR. Proc. Natl. Acad. Sci. U.S.A 2005;102:11167–11172. [PubMed: 16055561]
(26). Raviv U, Nguyen T, Ghafouri R, Needleman DJ, Li YL, Miller HP, Wilson L, Bruinsma RF, Safinya CR. Biophys. J 2007;92:278–287. [PubMed: 17028134]
(27). Huang, L.; Hung, M-C.; Wagner, E. Non-Viral Vectors for Gene Therapy. Vol. 2nd ed.. Vol. 53. Elsevier; San Diego: 2005.
(28). Ewert KK, Ahmad A, Evans HM, Safinya CR. Expert Opin. Biol. Ther 2005;5:33–53. [PubMed: 15709908]
(29). Schnur JM. Science 1993;262:1669–1676. [PubMed: 17781785]
(30). Singh A, Wong EM, Schnur JM. Langmuir 2003;19:1888–1898.
(31). Shimizu T, Masuda M, Minamikawa H. Chem. Rev 2005;105:1401–1443. [PubMed: 15826016]
(32). Thomas BN, Safinya CR, Plano RJ, Clark NA. Science 1995;267:1635–1638. [PubMed: 17808182]
(33). Discher BM, Won YY, Ege DS, Lee JCM, Bates FS, Discher DE, Hammer DA. Science 1999;284:1143–1146. [PubMed: 10325219]
(34). Deming TJ. Nature 1997;390:386–389. [PubMed: 9389476]

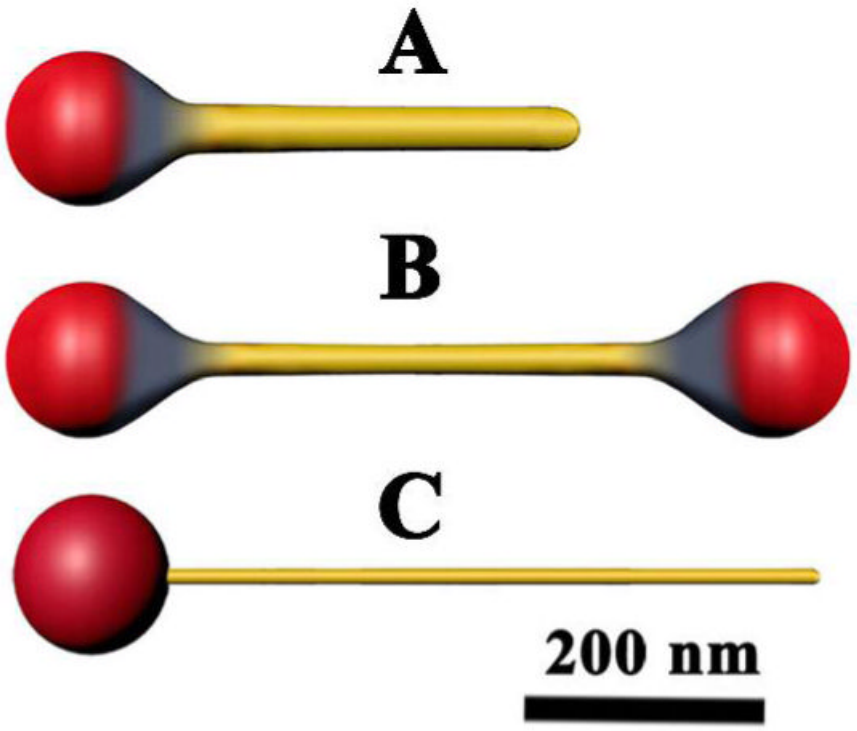

Figure 1. Block Liposomes (BLs)

Cryo-TEM reveals nanoscale block liposomes: (**A**) diblock (pear-tube), (**B**) triblock (pear-tube-pear) and (**C**) diblock (sphere-rod) liposome. The color coding represents different membrane Gaussian curvature: positive (red), negative (blue) and zero (yellow).

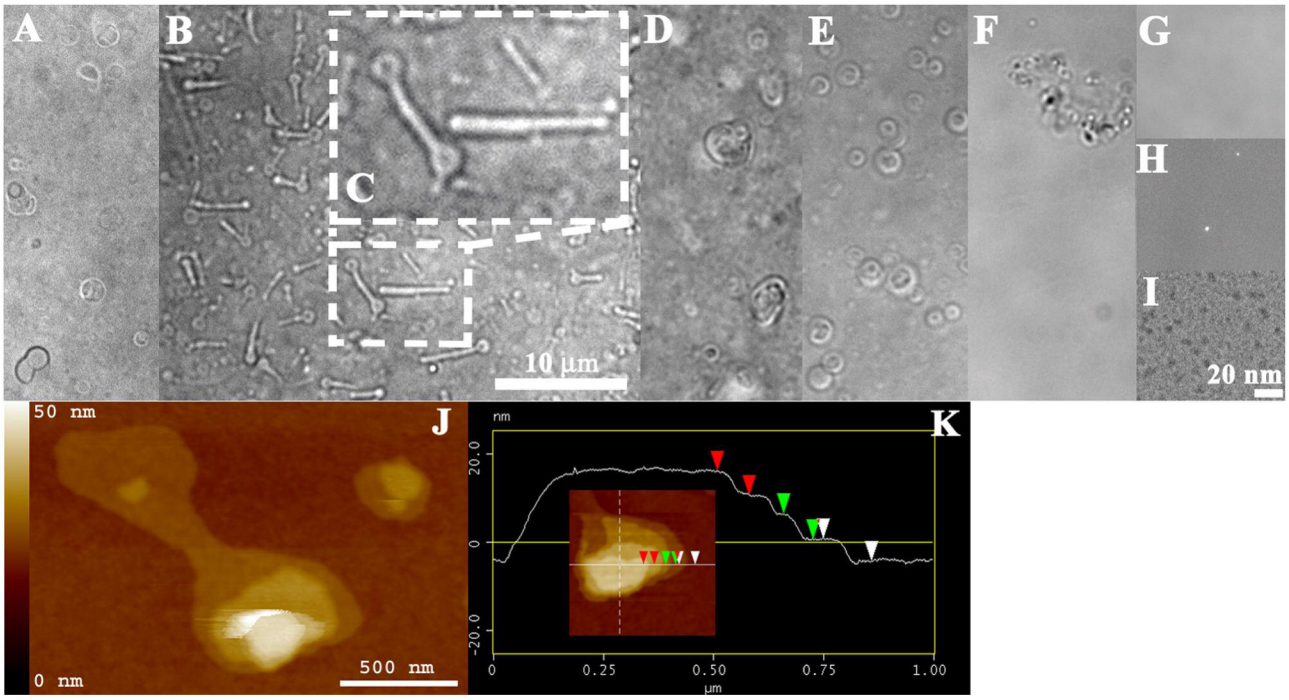

Figure 2. Phase behaviour of the MVLBG2/DOPC/water system

A-G, DIC images of vesicle shape transitions as a function of their composition: onions (0-8 mol % MVLBG2, **A**), novel block liposomes (8-10 mol % MVLBG2, **B**), reentrant onions (11-50 mol % MVLBG2, **D, E**), macroscopic coexistence of vesicles and micelles (≈50 mol % MVLBG2**, F**) and micelles (75-100 mol % MVLBG2, **G**). Fluorescence microscopy shows existence of micelles (**H**), cryo-TEM their size and morphology (**I**). **C**, An inset of (**B**), shows the block liposome morphology in detail; ≈5 μm long cylindrical core of diameter ≈0.5 μm capped with spherical vesicles with diameter of a few μm at both ends. **J**, AFM image of a triblock liposome. **K**, AFM height analysis shows multilamellar structure of the triblock.

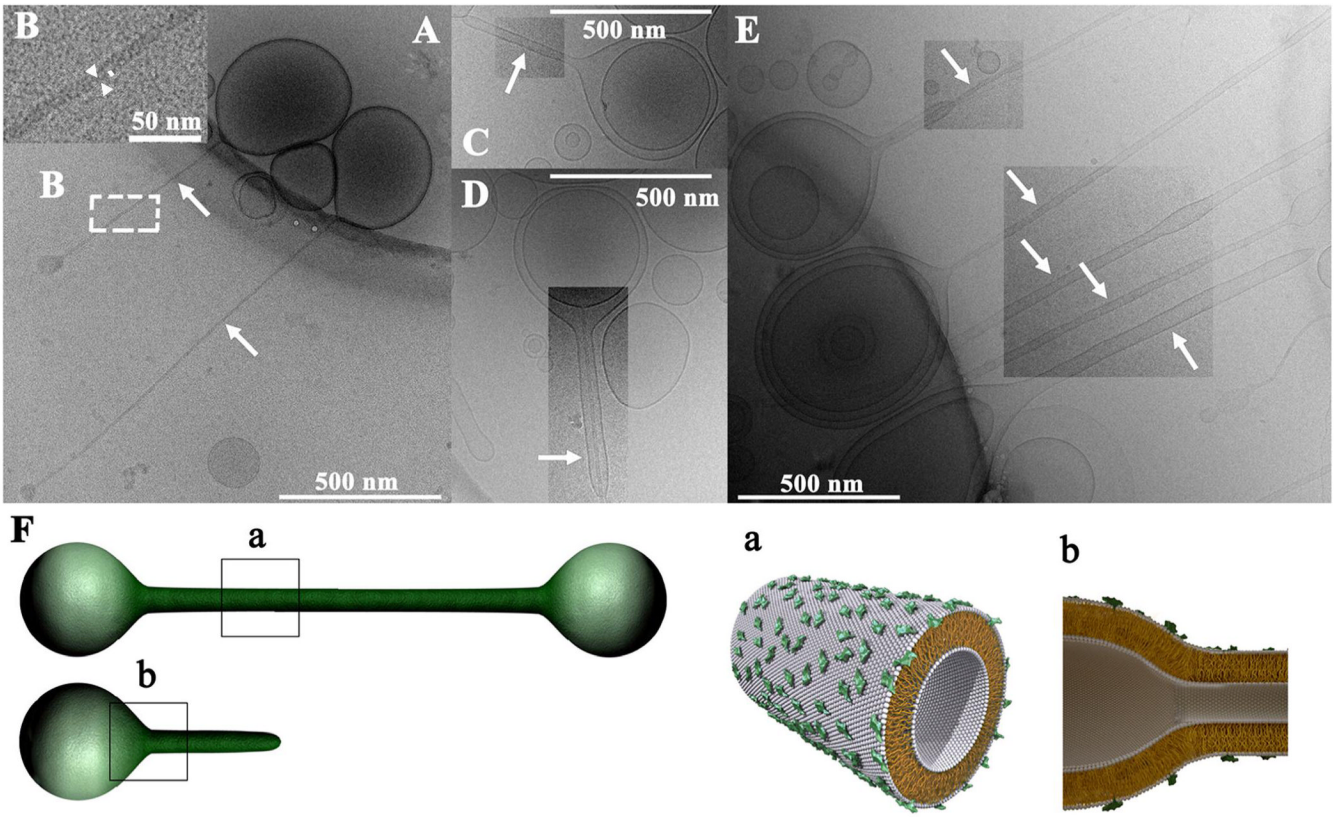

Figure 3. Cryo-TEM images of block liposomes containing liquid-phase lipid nanotubes

A, Triblock liposomes (pear-tube-pear). **B,** an inset of **A** disclosing the hollow tubular structure (white arrowheads and white bar point out the bilayer thickness of 4 nm). **C**, A diblock liposome. **D**, One block liposome encapsulated within another one (also seen in **E**, top arrow). **E**, A group of block liposomes. Block liposomes shown in **A-E** are comprised of liquid-phase lipid nanotube segments capped by spherical vesicles with diameters of a few hundred nm. The nanotubes (white arrows) are 10-50 nm in diameter and >1 μm in length. **F**, Schematics of the MVLBG2/DOPC tri- and diblock liposomes. **a** and **b** show molecular-scale illustrations, based on the hypothesized mechanism of their formation (cf. Fig. 5), manifesting the symmetry breaking between outer and inner monolayer. In **A-E**, image contrast/brightness was altered in selected rectangular areas. See the SI for untreated images.

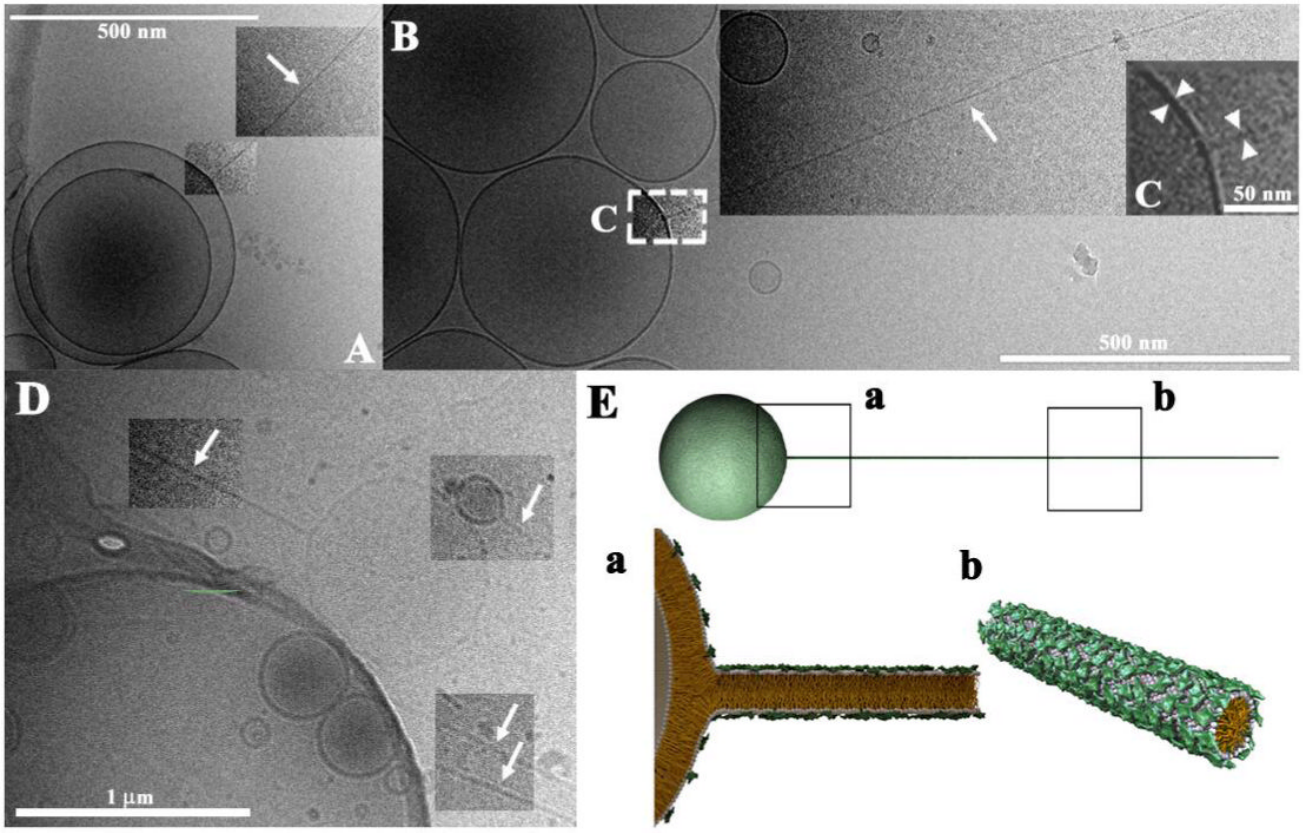

Figure 4. Cryo-TEM images of block liposomes containing liquid-phase lipid nanorods

A-D, Diblock liposomes comprised of lipid nanorods (white arrows) connected to spherical vesicles. In all images analyzed (426) no cases of free nanorods were found. Lipid nanorods are stiff cylindrical micelles with an aspect ratio ≈1000. Their diameter equals the thickness of a lipid bilayer (≈4 nm) and their length can reach up to several μm with a persistence length of the order of mm. **C** (an inset of **B**) demonstrates the thickness of the nanorod: white arrow heads point out a thickness of ≈4 nm (approximate bilayer thickness, identical for the spherical vesicle and the nanorods). **E**, Schematic of a MVLBG2/DOPC diblock comprised of a lipid nanorod attached to a vesicle. Insets **a** and **b** show molecular-scale schematics based on the hypothesized mechanism of formation (cf. Fig. 7). Note the high concentration of MVLBG2. In **A-D,** image contrast/brightness was altered in selected rectangular areas. See the SI for untreated images.

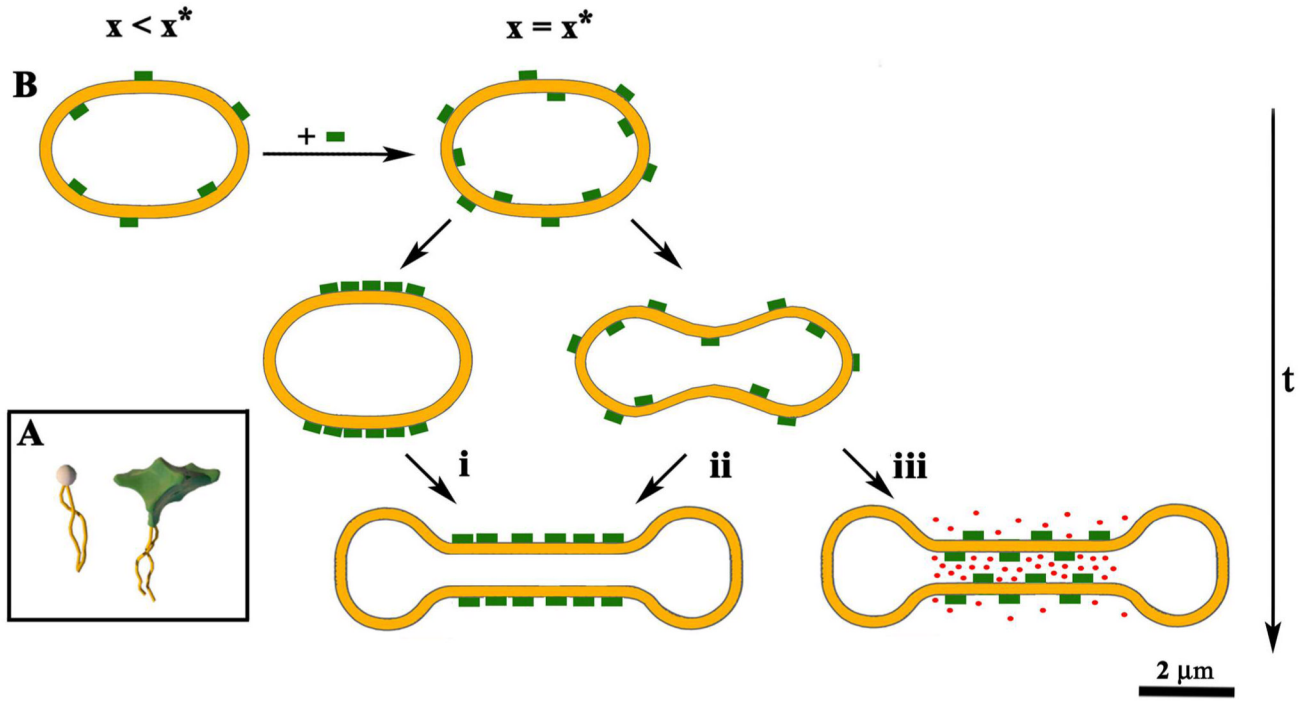

Figure 5. Model of Formation of Block Liposomes

A, Schematic of DOPC (white) and MVLBG2 (green) molecules. **B**, Illustration of flow of vesicle shapes leading to block liposome formation via a compositional fluctuation leading to a region with a high concentration of MVLBG2 (green), coupled to a curvature fluctuation (**i**); or a bending mode fluctuation producing a high curvature region coupled to either a compositional fluctuation (**ii**), or a non-symmetrical distribution of counterions between the outside and the inside of the bilayer (**iii**). Green blocks represent MVLBG2-distribution in membrane, red dots represent counterions, x is MVLBG2 mole fraction, x* is the mole fraction in the block liposome regime.

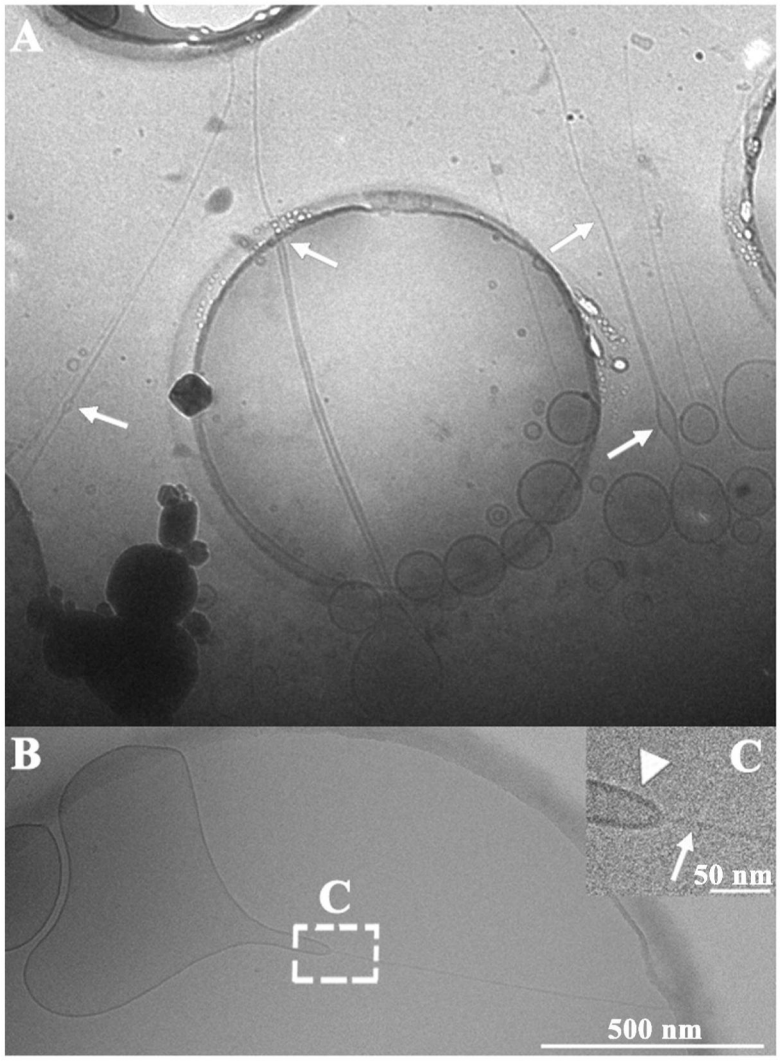

Figure 6. Nanotube-nanorod transition

A, Cryo-TEM image of a population of nanotubes and nanorods. White arrows indicate loci of the nanotube-nanorod transition with drastic change in diameter. **B**, Cryo-TEM of a locus of the nanotube-nanorod transition. **C**, An inset of **B** (white arrowhead highlighting nanotube, white arrow highlighting nanorod).

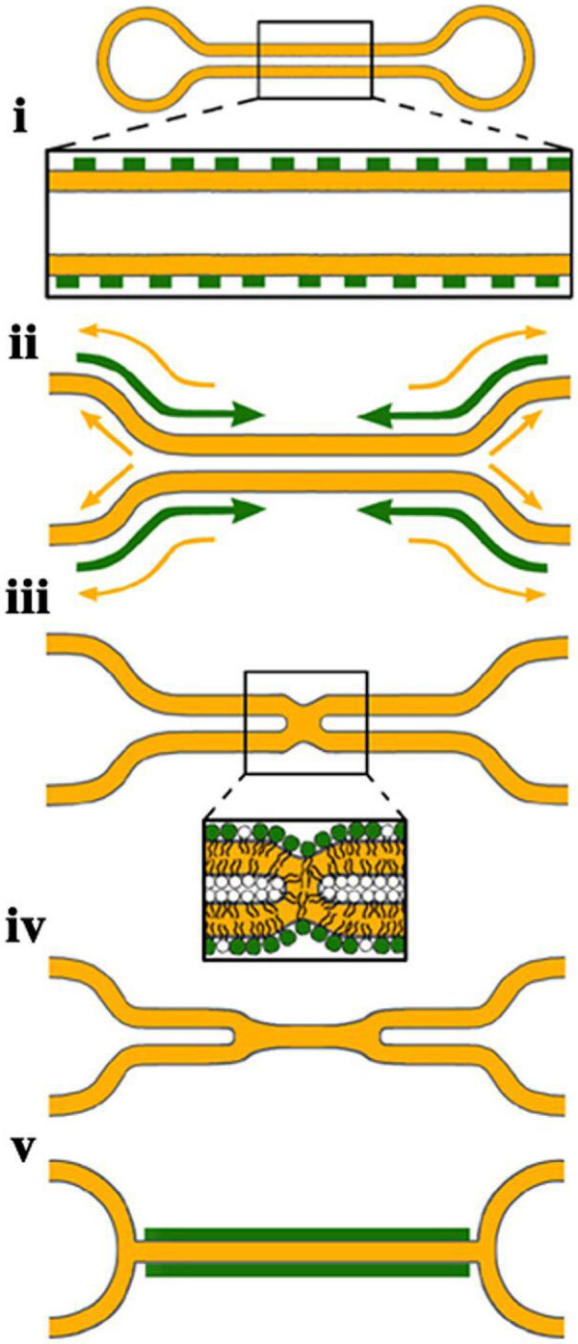

Figure 7. Model of the nanotube-nanorod transition

MVLBG2 is originally homogeneously distributed in the outer monolayer of the nanotube (**i**), a fluctuation brings the opposite walls closer, generating a higher curvature region and thus inducing a lateral phase separation (**ii**), the higher MVLBG2 concentration in the outer monolayer reduces the tube diameter, enabling nucleation of a nanorod (**iii**), nanorod formation proliferates (**iv**) until all MVLBG2 is used (**v**).

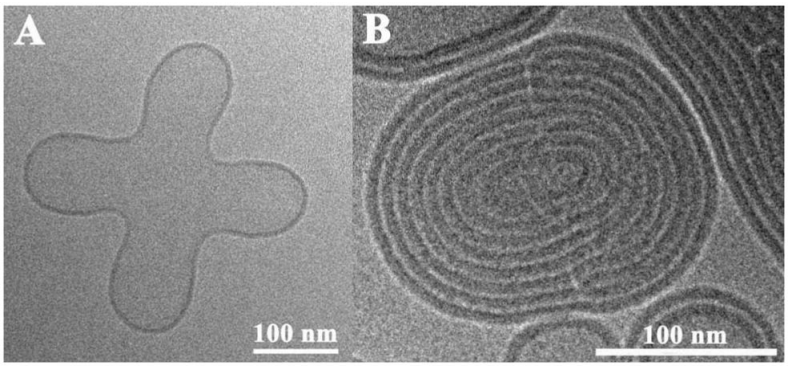

Figure 8. Cryo-TEM images of block liposomes

A, an example of four simultaneous nanotube formation processes show that there is no preferred orientation. **B**, when the electrostatic forces are screened by presence of salt (250 mM NaCl, Debye length ≈0.6 nm), block liposomes transform into regular multilamellar spherical vesicles.

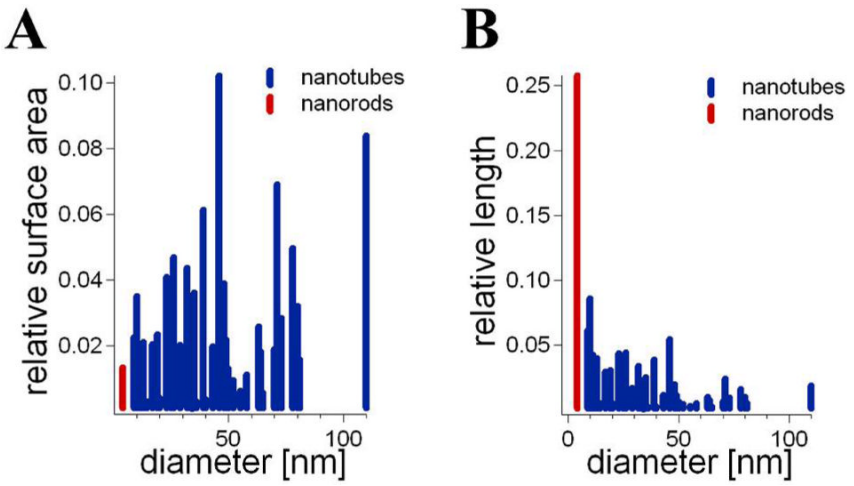

Figure 9. Statistical analysis of the nanotube and nanorod populations

A, Diameter histogram weighted by the surface area indicates the actual amount of material in the nanorod and nanotube state. **B**, Diameter histogram weighted by the length of the structure manifests the striking length of nanorods compared to nanotubes.